J Nanopart Res (2014) 16:2788
DOI 10.1007/s11051-014-2788-1

RESEARCH PAPER

Electrical conductivity, thermal conductivity, and rheological properties of graphene oxide-based nanofluids

Mahboobeh Hadadian · Elaheh K. Goharshadi · Abbas Youssefi

Received: 7 August 2014 / Accepted: 1 December 2014 / Published online: 11 December 2014

Abstract Highly stable graphene oxide (GO)-based nanofluids were simply prepared by dispersing graphite oxide with the average crystallite size of 20 nm, in polar base fluids without using any surfactant. Electrical conductivity, thermal conductivity, and rheological properties of the nanofluids were measured at different mass fractions and various temperatures. An enormous enhancement, 25,678 %, in electrical conductivity of distilled water was observed by loading 0.0006 mass fraction of GO at 25 °C. GO–ethylene glycol nanofluids exhibited a non-Newtonian shear-thinning behavior followed by a shear-independent region. This shear-thinning behavior became more pronounced at higher GO concentrations. The maximum ratio of the viscosity of nanofluid to that of the ethylene glycol as a base fluid was 3.4 for the mass fraction of 0.005 of GO at 20 °C under shear rate of 27.5 s^{-1}. Thermal conductivity enhancement of 30 % was obtained for GO–ethylene glycol nanofluid for mass fraction of 0.07. The measurement of the transport properties of this new kind of nanofluid showed that it could provide an ideal fluid for heat transfer and electronic applications.

Keywords Electrical conductivity · Viscosity · Thermal conductivity · Graphene oxide · Nanofluid

M. Hadadian · E. K. Goharshadi (✉)
Department of Chemistry, Ferdowsi University of Mashhad, Mashhad 91779, Iran
e-mail: gohari@ferdowsi.um.ac.ir

E. K. Goharshadi
Center of Nano Research, Ferdowsi University of Mashhad, Mashhad, Iran

A. Youssefi
Par-e-Tavous Research Institute, Mashhad, Iran

Introduction

Graphite oxide (GtO), a material first discovered by Benjamin Brodie in 1859 (Brodie 1860), has attracted recurring interest from the chemist community. Exfoliation of GtO produces monolayers of atomically thin graphene oxide (GO) sheets that are dispersible in basic media. GO is a heterogeneous compound consisting of graphene sheet covalently bonded to oxygen-bearing groups. The basal plane of GO is decorated with epoxy and hydroxyl functional groups, whereas carbonyl and carboxylic acid are attached to the edges (Kumar et al. 2014). The coverage of oxygen groups varies depending on the degree of oxidation in the preparation process.

GO possesses unique features such as large surface area, high water dispersibility, good colloidal stability, ability to easy surface modification, good biocompatibility, distinctive amphipathic nature, and superior mechanical properties (Yin et al. 2013). GO is prepared via a simple and low cost route using graphite, an abundant and inexpensive

natural source (Yin et al. 2013). The peculiar properties make GO to be a versatile, solution-processable candidate material for next-generation ultrathin optoelectronics (Loh et al. 2010), biodevices (Yin et al. 2013), and nanocomposites (Li et al. 2013). The amphipathic nature makes GO to be easily dispersed in lots of common solvents including water, ethylene glycol (EG), and ionic liquids (Wang et al. 2012a). These advantages suggest that this material can also perform as an excellent additive in nanofluid technology.

Nanofluid technology, a new interdisciplinary field of great importance, has largely developed over the past decade. Nanofluids, suspensions of nanometer-sized materials, have various superior properties compared with those of their base fluids (Goharshadi et al. 2013). The distinguished features of nanofluids make them potentially useful in a plethora of applications such as in cooling of electronic equipment, vehicle engines, nuclear reactors, biomedical engineering, and energy efficiency enhancement (Salehi et al. 2013).

Among all the physical properties of nanofluids, the thermal conductivity (TC) is the most important property for many applications. By suspending some nanomaterials in heating or cooling fluids, the heat transfer performance of the fluid can be improved significantly. A large number of investigations have been reported on TC of metal and metal oxide nanofluids both experimentally and theoretically (Abareshi et al. 2010; Moosavi et al. 2010; Patel et al. 2010). The nanofluids containing carbonaceous materials such as carbon nanotubes (CNTs) (Chen and Xie 2009), diamond nanoparticles (Yeganeh et al. 2010), graphene (Baby and Ramaprabhu 2010), and GO (Yu et al. 2010a) have attracted great interest because of their large intrinsic TC and low density compared with those of metals or metal oxides (Yu et al. 2010a). Yu et al. (2010a) reported the TC of GO–EG nanofluids. They observed an enhancement of 61 % for a loading of 5 vol% of GO nanosheets at room temperature. Later, the same group (Yu et al. 2010b) studied the TC of GO dispersion in distilled water, propyl glycol, and liquid paraffin. They reported the TC enhancement ratios of 30.2, 62.3, and 76.8 % for nanofluids (5 vol% GO loading) with distilled water, propyl glycol, and liquid paraffin as base fluid, respectively.

Electrical conductivity (EC) of a nanofluid is related to the ability of charged particles in the suspension to carry the charges toward respective electrodes when an electric potential is applied (Sarojini et al. 2013). The electrically conducting fluids have a variety of technological and industrial applications such as field-induced pattern formation in colloidal dispersion, sensors, and electrically conductive adhesive technology (Kolbe et al. 2007). EC of nanofluids containing metal, metal oxide, and CNT have been studied in the literature (Azizi-Toupkanloo et al. 2014; Goharshadi and Azizi-Toupkanloo 2013b; Sarojini et al. 2013). Baby and Ramaprabhu (2010) measured the electrical conductivity of graphene–water nanofluid with different volume fractions and at different temperatures. They observed an enhancement of about 1,400 % for a volume fraction of 0.03 % at 25 °C. To the best of our knowledge, the present research is the first work measuring the EC of aqueous suspension of GO nanosheets.

Rheological properties provide the knowledge on the microstructure under both static and dynamic conditions (Goharshadi and Azizi-Toupkanloo 2013b). One of the most important rheological measurements is determining the dynamic viscosity, which is an important transport property for applications of nanofluids in thermal devices such as heat exchangers or cooling systems. Researchers accomplished some works on the viscosity of different nanofluids focusing on the effective parameters like temperature, shear rate, and particle size, shape, and concentration (Azizi-Toupkanloo et al. 2014; Goharshadi and Hadadian 2012; Moghaddam et al. 2013; Ruan and Jacobi 2012). Tesfai et al. (2013) investigated the rheological properties of aqueous suspension of GO. They observed 470 % increase in viscosity of the nanofluid for 0.5 mg/ml GO loading at a shear rate of 2.5 s^{-1}.

The first aim of the present work was to fabricate GtO using modified Hummers' method. The prepared sample was characterized by different techniques. Stable and well-dispersed GO–distilled water and GO–EG nanofluids with different mass fractions were prepared by exfoliation of GtO in the base fluids. Measurement of three transport properties including EC, TC, and viscosity of the prepared nanofluids as functions of mass fraction and temperature constituted the second goal of this study.

Materials and methods

Materials

All chemicals including graphite powder (<0.1 mm and >95 %), sulfuric acid (H_2SO_4), sodium nitrate ($NaNO_3$), potassium permanganate ($KMnO_4$), hydrogen peroxide (H_2O_2), hydrogen chloride (HCl), and EG were of analytical grade and used as received without further purification.

Synthesis of GtO

GtO was synthesized from parent graphite powder using modified Hummers' method (Wu et al. 2009). Typically, graphite powder (2 g) was mixed with 70 ml concentrated H_2SO_4 (95 %) and 0.024 mol $NaNO_3$ for 15 min while being cooled in an ice water bath. Subsequently, 0.038 mol potassium permanganate was gradually added into the mixture. The suspension was stirred for 15 min at 0 °C. The color of the mixture turned to green due to the presence of oxidizing agent (MnO^{3+}). The ice bath was removed and the mixture was allowed to stand for 48 h at room temperature with gentle stirring. Subsequently, 92 ml deionized water was slowly added to the obtained brown pasty mixture for 10 min. Then, the suspension was diluted by 200 ml of warm water (35 °C) and treated with 70 ml of H_2O_2 (30 wt%) for 30 min. By this treatment, residual permanganate reduced to soluble manganese ions (Wu et al. 2009). The resulting solid was centrifuged and washed several times with HCl (5 wt%) and deionized water. In order to ensure that SO_4^{2-} and Cl^- were completely removed, the supernatant was tested by $BaCl_2$ and $AgNO_3$, respectively. Finally, it was dried at 60 °C in vacuum oven overnight.

Nanofluid preparation

To prepare GO-based nanofluids with various mass fractions, different masses of GtO were added to 50 ml of the base fluids (distilled water and EG). The suspensions were subjected to ultrasonic vibration for 15 min at 25 °C to exfoliate GtO and obtain uniform dispersions of GO. Using mass fraction in preparing nanofluids seems to be more appropriate than using volume fraction because the precise density value of GO is not available.

Instruments

The chemical composition of GtO was analyzed using Thermo Finnigan (Flash 1112 Series EA) CHN analyzer based on the burn-off mass of the sample. The X-ray diffraction (XRD) pattern of sample was determined by means of a Bruker/D8 Advanced diffractometer in the 2θ range from 5° to 65°, by step of 0.04 degree, with graphite monochromatic Cu Kα radiation ($\lambda = 1.541$ Å).

The transmission electron microscope (TEM) used for analysis of the sample was a Philips CM120 TEM with a maximum acceleration voltage of 120 kV. Morphology observations were performed on a field emission scanning electron microscope (FESEM), Hitachi S4160 operated at 15 kV. The Fourier transform infrared (FTIR) spectrum was recorded at room temperature on Thermo Nicolet Avatar 370 FTIR Spectrometer ranging from 500 to 4,000 cm^{-1}. Raman spectrum of the sample was recorded using an Almega Thermo Nicolet Dispersive Raman Spectrometer with an excitation energy of 2.33 eV (532 nm, Nd:YLF laser source). The sample was deposited on silicon wafer in powder form without using any solvent. The UV–Vis absorption spectrum was obtained for the samples using an Agilent photodiode-array Model 8453 equipped with glass of 1 cm path length. The spectrum was recorded at room temperature within the wavelength range of 200–800 nm.

Sonicator 4000 (20 kHz) with total power of 50 W was used for dispersing GtO in order to make GO suspensions. The zeta potential of GO–distilled water nanofluid was measured by the Zeta sizer (Nano-ZS) from Malvern instrument.

The EC of the GO–distilled water nanofluids (stationary) was measured using an EDT instrument BA 380 (DC 9 V 0.5 W) with accuracy of ±1 %. The measurements were performed in the range of 0.1 μS/cm–200 mS/cm. The measuring cell was connected to a circulating cooling water bath (BL 7100, Major Science) to control the water temperature. The viscosity of GO–EG nanofluid was measured using a Brookfield rheometer (LV DV-II + ProEXTRA) with a sample adaptor. It contains a cylindrical sample holder equipped with a water jacket connected to a

circulating cooling water bath to control the water temperature. The TC was measured using the KD2 Pro Thermal Properties Analyzer (Decagon Devises, Inc.). KD2 Pro is based on the well-known transient hot wire method. The sample container was connected to a circulating water bath (Thermo Haake K10) to ensure the measurements were done at constant temperatures.

Results and discussion

Characterization

CHN elemental analysis was carried out to evaluate the chemical composition of the sample. It showed that GtO was composed of approximately 44.7 wt% carbon and 2.5 wt% hydrogen. The oxygen content can be estimated as a difference between 100 % and the sum of C+H, assuming that ash is not present (Long et al. 2010; Sun et al. 2012). The GtO prepared in this work contains approximately 52.8 wt% oxygen. Hence, the atomic ratio of carbon to oxygen (C_{at}/O_{at}) is ca. 1.13.

The XRD pattern of GtO shows a strong peak at $2\theta = 11.6^{\circ}$ attributed to the (002) crystalline plane (Fig. 1a). The corresponding interlayer spacing of GtO (0.76 nm) was larger than that of pristine graphite (0.34 nm) (El Achaby et al. 2012; Lee et al. 2012) indicating the full oxidation of graphite. During oxidation of graphite, oxygen-containing functional groups are introduced into the basal plane and the edge of its structure. Therefore, water can be intercalated within the lamellar structure of GtO and results in a large basal spacing compared to pristine graphitic structure. The value of basal spacing depends on the amount of water within the GtO structure. Consequently, different 2θ values, ranging from 10° to 12.4°, were reported for GtO in the literature (Lee et al. 2012; Shao et al. 2012; Wang et al. 2012b).

FTIR spectrum was employed to explore the functional groups on GtO. The FTIR spectrum of GtO shown in Fig. 1b confirms the successful oxidation of the graphite. The spectrum displays a broad peak at 3,401 cm^{-1} attributed to O–H stretching vibrations of adsorbed water molecules and structural OH groups (Wang et al. 2012b). The most recognizable features in the most reported IR spectra of GtO are two bands in the middle of the spectrum. One is the band around 1,722 cm^{-1} which is unambiguously assigned to C=O stretching of carbonyl group. The other band appears around 1,617 cm^{-1}. Some researchers attributed this band to the aromatic C=C bond (El Achaby et al. 2012), while others assigned it to water bending modes (Wojtoniszak and Mijowska 2012). The presence of epoxy functional groups could be detected at around 1,226 and 1,053 cm^{-1} (Chen et al. 2010).

Raman spectroscopy as a powerful and non-destructive tool has historically played an important role in the structural characterization of graphitic materials. Figure 1c shows the Raman spectrum of GtO. There are two main prominent peaks for GtO assigned to G band (1,597 cm^{-1}) and disorder-induced D band (1,358 cm^{-1}). These bands are present in all polyaromatic hydrocarbons. G band originates from the in-plane vibration of sp^2 carbon atoms and is a doubly degenerate phonon mode (E_{2g} symmetry) at the Brillouin zone center. The G band is always in the range 1,500–1,630 cm^{-1}. The D band is a defect-induced breathing mode of A_{1g} symmetry involving phonons near the K zone boundary (Moghaddam et al. 2013). This mode is forbidden in perfect infinite graphite and becomes active in the presence of disorder. The D mode exhibits a dispersive behavior i.e., its frequency in the Raman spectra changes as a function of the energy of the incident laser (Malard et al. 2009). The G band of GtO shifts toward a higher wavenumber with respect to that of graphite (1,575 cm^{-1}). It may be due to the oxidation of graphite and the formation of new sp^3 carbon atoms, defects, and disorder in the graphite lattice (Krishnamoorthy et al. 2013). In addition to G and D bands, there were three other Raman bands with weaker intensity, called 2D (2,740 cm^{-1}), D+G (2,950 cm^{-1}), and 2G (3,182 cm^{-1}). The 2D band is the overtone of the D band. Some authors prefer to call it the G' band because this band is symmetry-allowed and appears in the second-order Raman spectra of crystalline graphite (without any kind of disorder) (Pimenta et al. 2007). Similar to the D band, 2D peak position is also dispersive (Malard et al. 2009). The 2G band is the overtone of the G mode, while D+G is the combination mode induced by disorder (Pimenta et al. 2007).

It is known that a ratio between the intensity of D and G bands (I_D/I_G) is a measure of disorder and determines the relative defect content (Wojtoniszak and Mijowska 2012). Here, the value of I_D/I_G was approximately 0.96. This ratio depends not only on the amount of disorder but also on the excitation

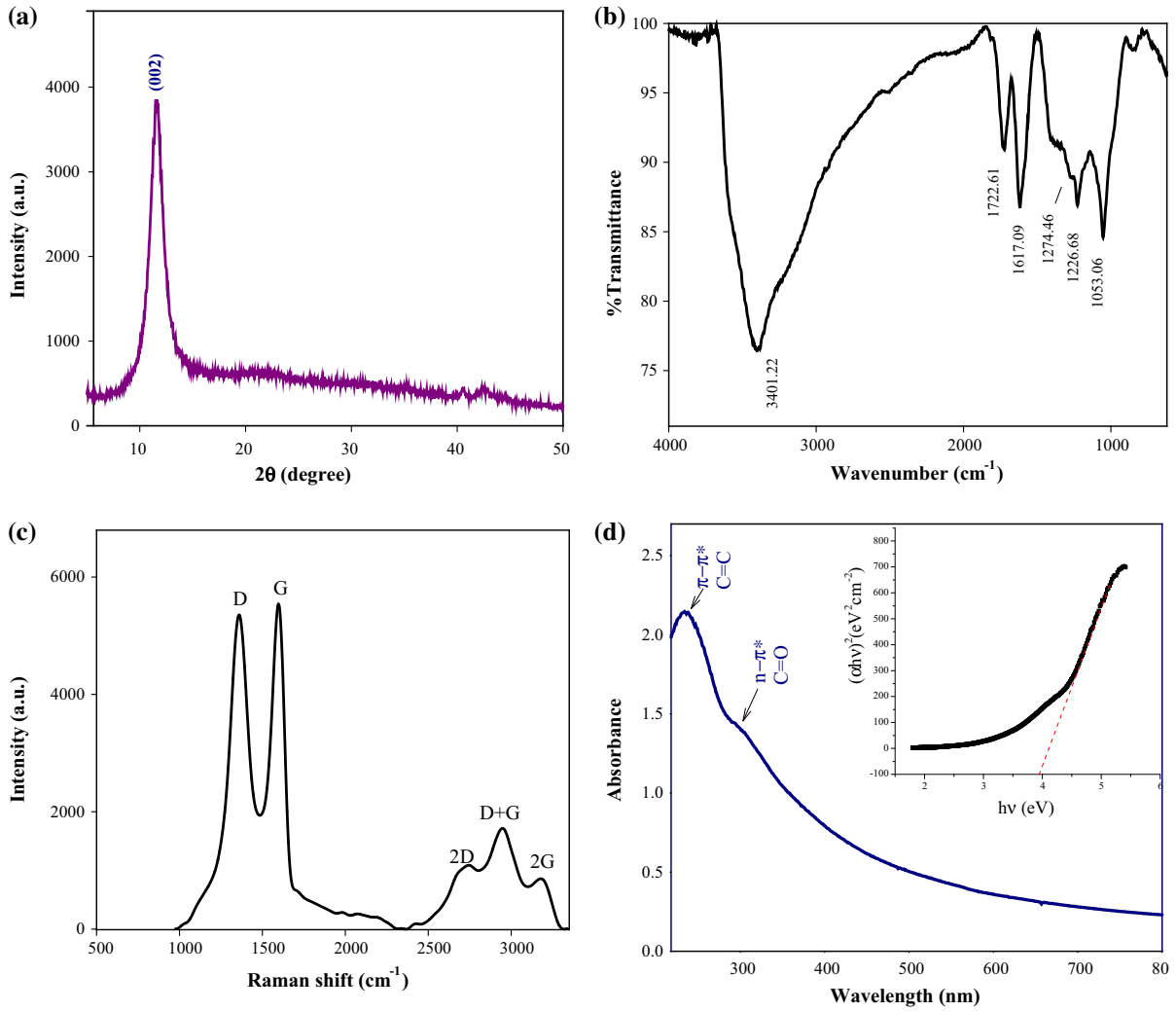

Fig. 1 **a** XRD pattern, **b** FTIR spectrum, and **c** Raman spectrum of GtO. **d** UV–Vis absorption spectrum of aqueous GO suspension (Plot of $(\alpha h\upsilon)^2$ versus photon energy is shown in the *inset*)

laser energy. Tuinstra (1970) performed systematic Raman and XRD studies of many graphitic samples with different average crystallite sizes, L_a. They concluded that this ratio is inversely proportional to the average crystallite size. The general equation of L_a was given by Cancodo et al. (2006) using the I_D/I_G ratio and the fourth power of the excitation laser energy in eV, E_{Laser}, used in the Raman experiment:

$$L_a(nm) = \frac{560}{E_{Laser}^4}\left(\frac{I_D}{I_G}\right)^{-1}. \quad (1)$$

Considering the laser line wavelength (λ_{Laser}) in nm units, Eq. (1) can be rewritten as

$$L_a(nm) = \left(2.4 \times 10^{-10}\right)\lambda_{Laser}^4\left(\frac{I_D}{I_G}\right)^{-1}. \quad (2)$$

The value of L_a for GtO in this work was calculated to be 20.11 nm.

The UV–Vis absorption spectrum recorded for aqueous GO dispersion is shown in Fig. 1d. The absorption spectrum exhibited a maximum peak at 234 nm corresponding to π–π* transition of conjugation system in the polyaromatic structures. A small

shoulder at 300 nm which is due to n–π^* transition of carbonyl groups was also observed (Marcano et al. 2010). The absorption peak of GO related to conjugation system showed blue shift when compared with that of graphene (270 nm). Reduction of electronic conjugation during oxidation of graphite causes the HOMO and LUMO to be further away in GO and results in a lower λ_{max} (Kumar et al. 2013).

The band gap energy, E_g, was estimated from UV–Vis absorption using Tauc's equation (Goharshadi and Hadadian 2012):

$$(\alpha h\upsilon)^n = B(h\upsilon - E_g), \quad (3)$$

where α, $h\upsilon$, and B are absorption coefficient, photon energy, and a constant relative to the material, respectively. The parameter n represents the nature of optical transition, $n = 2$ for direct transitions and $n = 1/2$ for indirect transitions. Plotting $(\alpha h\upsilon)^n$ against the photon energy and extrapolating the linear region of the curve to the x-axis give the optical band gap. The variation of $(\alpha h\upsilon)^2$ with photon energy for aqueous GO dispersion is shown as the inset of Fig. 1d. The estimated band gap of GO was calculated to be 3.95 eV. Of course, Tauc's relation has some limitations. First, it is valid in a relatively narrow energy range corresponding to the region of parabolic bands where a sharp increase of the optical transmission is detectable experimentally (Amato 1991). Second, Tauc's plot overestimates slightly band gap in a reflection type of measurement such as spectroscopic ellipsometry (Radović et al. 2013). Finally, there is ambiguity on the energy range that the Tauc's extrapolation is correct (Solomon et al. 1988).

Understanding the electronic band structure of GO is complicated due to its large structural and chemical inhomogeneity. Different factors such as oxidation degree and time can influence the structural and optical properties of GO. Therefore, different band gap energies were reported for GO in the literature. In general, for non-stoichiometric and hygroscopic compounds like GO, a linear increase of the band gap with an increase in oxygen to carbon ratio has been established (Acik and Chabal 2012; Boukhvalov and Katsnelson 2008; Jung et al. 2009).

Figure 2a shows a typical TEM of GO. In order to perform TEM analysis, GtO powder was dispersed in deionized water under sonication. The figure clearly illustrates well-exfoliated and large surface area GO which was folded in some regions. It also shows that GO consisted of few-layer thick and transparent nanosheets. The FESEM image of GtO (Fig. 2b) shows that GtO was composed of paper-like layers with different sizes. It also illustrates that stacking of the sheets was substantially disordered.

Stability of dispersions

Aqueous suspension of GO is highly stable with no coagulation for a long time. Lerf–Klinowski model (Lerf et al. 1998) proposes that GO consists of two different randomly distributed domains: aromatic region of pure graphene with sp^2 hybridized carbon atoms and areas of oxidized or sp^3 hybridized carbon atoms. The oxidized domains result in the polar surface properties and excellent hydrophilicity of GtO.

The stability of GO–distilled water dispersions is due to the electrostatic or charge stabilization. The origin of the surface charge is due to the deprotonation of surface acidic groups. One of the peculiar properties of GO is the high acidity of its aqueous solutions (pH $\sim$3) (Dimiev et al. 2012). The first evidence for the presence of acidic groups was the change of pH of the nanofluid with mass fraction, f_m. For investigating this evidence, the GO aqueous suspensions with different mass fractions were prepared using sonication (Fig. 3a), and the pHs were measured (Fig. 3b). As the figure shows, by increasing the mass fraction from 0.0001 to 0.0006, pH decreased from 2.96 to 2.66. The increase in acidity of the suspension by increasing GO loading indicates that more number of protons (H^+) are released through deprotonation of surface acidic groups. The second evidence for the deprotonation of GO was the evolution of pH with time during the preparation of the suspension (Fig. 3c). In order to investigate the second evidence, the GO–distilled water suspension ($f_m = 0.0003$) was prepared by magnetic stirring instead of sonication. It is impossible to read pH during the sonication because of the possibility of damaging the pH meter electrode. Decreasing the pH with time indicates that the deprotonation of surface acidic groups occurs. The deprotonation was faster within the first few seconds because more acidic groups were available. Then, it reduced until reaching a constant value. The feasibility of forming stable GO dispersions through electrostatic stabilization was examined by the zeta potential

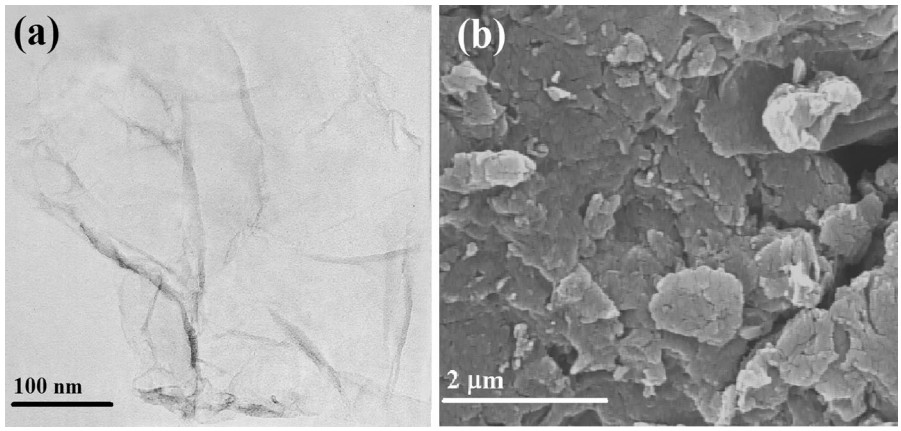

Fig. 2 **a** TEM image of GO and **b** FESEM picture of GtO

analysis. The zeta potential values more negative than −30 mV or more positive than +30 mV are generally considered to represent sufficient mutual repulsion to ensure the stability of a dispersion. Concerning the GO/water interface, it is known that GO nanosheets have negative charges when they are dispersed in water (Park and Ruoff 2009). As shown in Fig. 3d, zeta potential of GO–distilled water nanofluid at pH range between 3 and 10 was highly negative revealing strong repulsive forces between GO nanosheets. GO–distilled water nanofluid at pH = 3 exhibited zeta potential of −45.4 mV indicative of good stability of the suspension. The electrostatic repulsion between ionized carboxyl groups at the edge of GO nanosheets provides the major barrier preventing the GO sheets from aggregating (Shih et al. 2011). The negative zeta potential value indicates that the surface charges are negative. The surface charge depends upon the degree of deprotonation of the GO acidic functional groups (Goncalves et al. 2009; Shih et al. 2011). The ratio of C_{at}/O_{at} (estimated by XPS or CHN analysis) determines the number of acidic functional groups. It may correlate with the zeta potential—the greater the value of this ratio, the more the positive zeta potential (Kang and Shin 2012).

The aqueous suspensions of the prepared GO were stable for more than 5 months without any sedimentation (inset of Fig. 3d). The stability of aqueous dispersion of GO (0.01 mg/ml) was examined by UV–Vis spectroscopy (Fig. 3e). The absorbance at the wavelength of 228 nm was plotted against time during 60 days. The absorbance had no significant change which also confirmed the high stability of the suspension.

Electrical properties

The EC of GO–distilled water nanofluids was measured as a function of GO mass fraction, at different temperatures (Fig. 4a). The EC of distilled water was 0.9 µS/cm at room temperature.

As GtO is dispersed in distilled water, the nanosheets gain negative charges due to the deprotonation of surface functional groups (White et al. 2011). The negative surface charge is proved by the negative value of zeta potential (−45.4 mV). The ions with opposite charge are attracted to the surface, and the charged diffuse layer is formed. This layer together with the surface charge constitutes electrical double layer (EDL) which would vigorously contribute to the conduction through electrophoretic mobility (Shen et al. 2012).

As Fig. 4a shows, the EC of nanofluid increased linearly with increasing mass fraction and it reached to about 232 µS/cm for a mass fraction of 0.0006 at 25 °C. No leveling off in EC of the present nanofluids by increasing mass fraction was observed. The leveling off is due to the counter-ion condensation effect, indeed, it happens at high mass fractions (White et al. 2011). The mass fraction of GO–distilled water nanofluid in this work was very low.

The EC increased exponentially with temperature (Fig. 4b). The electrophoretic mobility of charged particles, μ_i, which determines the EC of a nanofluid

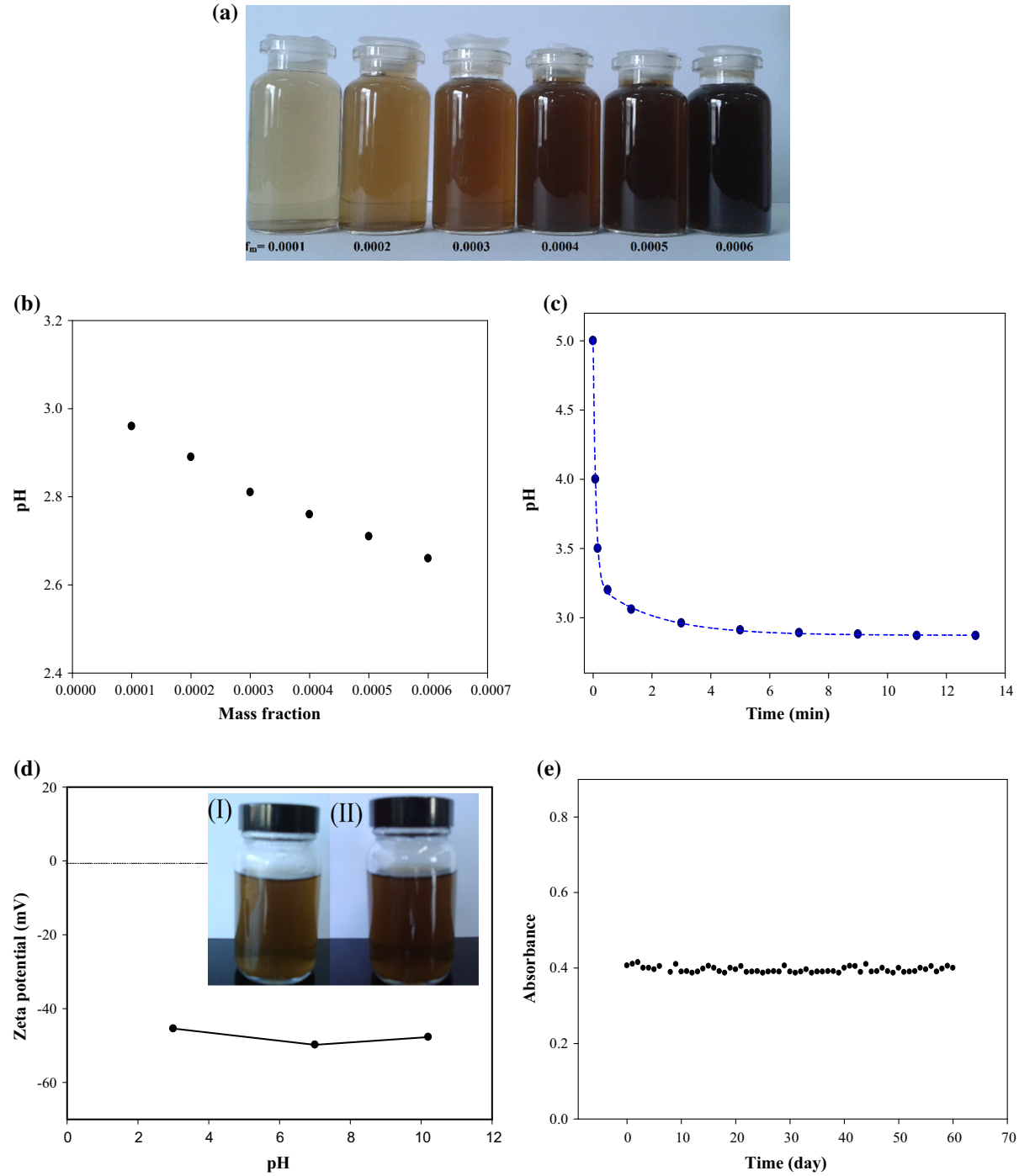

Fig. 3 **a** Digital photo of GO–distilled water nanofluids with different mass fractions. **b** pH values of GO–distilled water nanofluids at different mass fractions. **c** Variation of pH with preparation time for GO–distilled water nanofluids ($f_m = 0.0003$). **d** Zeta potential of GO–distilled water nanofluid with mass fraction of 0.0003 as a function of pH. The *inset* shows photographs of GO–distilled water nanofluid with mass fraction of 0.0003 (I) immediately after sonication and (II) 4 months after sonication. **e** Absorbance of aqueous suspension of GO at its λ_{max}(228 nm) over a period of 60 days at ambient temperature

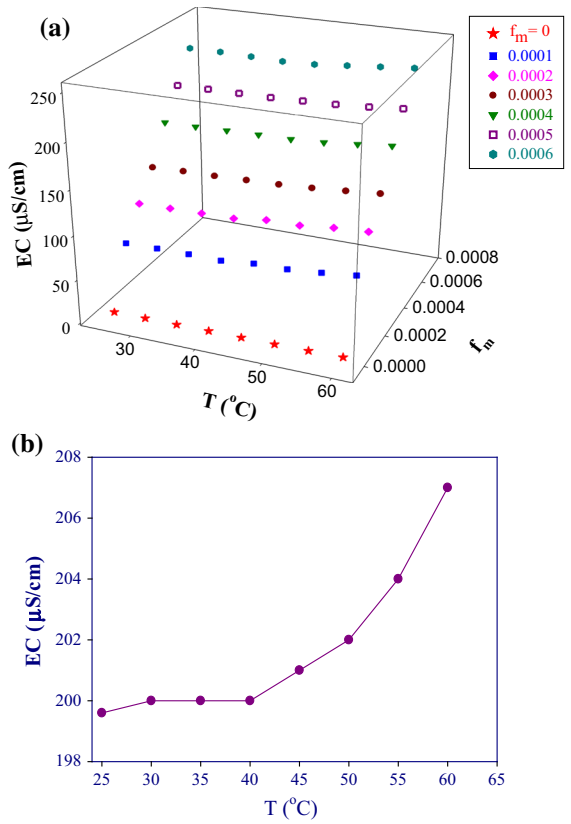

Fig. 4 **a** EC of GO–distilled water nanofluid as a function of temperature and mass fraction (zero mass fraction means distilled water) and **b** EC of GO–distilled water nanofluid versus temperature for mass fraction of 0.0005

(Sarojini et al. 2013) has reciprocal relationship with viscosity:

$$\mu_i = \frac{Q_{eff}}{6\pi\eta r}, \tag{4}$$

where Q_{eff} and r are effective charge and total radius of the ions, respectively. On the other hand, based on Arrhenius-like equation, the viscosity of fluid, η, decays exponentially with temperature:

$$\eta = C \exp\left(\frac{E_A}{RT}\right), \tag{5}$$

where E_A, T, C, and R are activation energy for the viscous flow, temperature, a constant, and molar gas constant, respectively. As the temperature increases, the viscosity of the fluid tends to decrease exponentially, and electrophoretic mobility rises exponentially. Therefore, EC shows an exponential growth by temperature.

A critical parameter affecting the electrophoretic mobility is EDL thickness. According to the Derjaguin–Landau–Verwey–Overbeek theory (Hunter 1981), the thickness of EDL varies inversely with the absolute temperature. By increasing the temperature, the EDL thickness decreases which has a positive effect on the enhancement of the EC of the nanofluid (Goharshadi and Azizi-Toupkanloo 2013b).

The agglomeration of the nanomaterials is an important factor that may affect the electrical conductivity of the suspensions (Ganguly et al. 2009). Formation of aggregates decreases the effective number of charge carriers due to reduction of the number density of the particles in the system. Therefore, it tends to reduce the electrical conductivity of the suspension (Ganguly et al. 2009). On the other hand, the aggregation leads to an enlargement of the particle size which has negative impact on both Brownian motion and electrophoretic mobility of nanomaterials in the suspension. Hence the electrical conductivity reduces (Dong et al. 2013; Sarojini et al. 2013). Since our prepared nanofluids were stable during several months, it is plausible to say that agglomeration was not formed to affect the value of the electrical conductivity.

The EC enhancement percentage of a nanofluid is defined as (Baby and Ramaprabhu 2010)

$$\text{EC enhancement}\,\% = \frac{\sigma - \sigma_o}{\sigma_o} \times 100, \tag{6}$$

where σ and σ_o correspond to ECs of the nanofluid and the base fluid, respectively. EC enhancement was plotted versus mass fraction for different temperatures (Fig. 5). It is obvious that the EC enhancement increased with mass fraction and decreased with temperature. Maximum enhancement of about 25,678 % in EC of distilled water was observed for mass fraction of 0.0006 of GO at 25 °C. As temperature increased for a certain mass fraction, the EC increased while its enhancement percentage decreased. The EC of the nanofluid with mass fraction of 0.0006 increased from 232 to 240 μS/cm by increasing temperature from 25 to 60 °C, while its enhancement decreased from 25,678 to 8,789 %.

A variety of equations have been suggested for description of the EC of the suspensions (Carrique and Ruiz-Reina 2009; White et al. 2011). Maxwell (1904) proposed the first model for predicting EC of liquid–solid suspensions. This model predicts the experimental

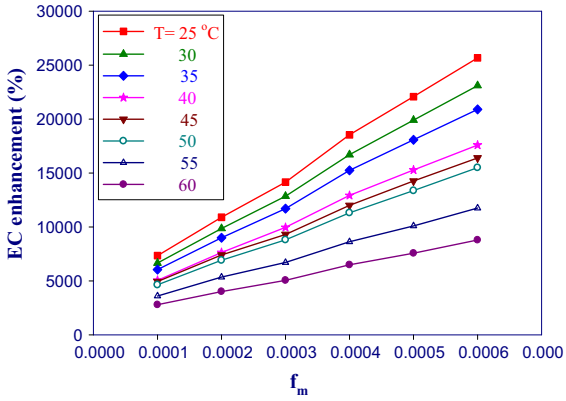

Fig. 5 EC enhancement percentage of GO–distilled water nanofluids as a function of mass fraction at different temperatures

data of dilute suspensions consisting of spherical microparticles (Ganguly et al. 2009). In the case of suspensions containing nanoparticles, this model underestimates the experimental values of EC (Ganguly et al. 2009; Sarojini et al. 2013) because it does not consider all the parameters affecting the EC of nanofluids such as EDL thickness, ionic strength, particle size, and surface charge (Chakraborty and Padhy 2008). Some researchers attempted to develop some models by considering the neglected parameters in Maxwell model (Chakraborty and Padhy 2008; White et al. 2011). Although the proposed models reproduce experimental data of spherical colloidal particles, they cannot be applied for nanofluids containing sheet-like nanomaterials such as GO.

In this study, a simple empirical equation was developed for the EC of GO–distilled water nanofluids as a function of mass fraction for all temperatures:

$$\sigma = \alpha + \beta f_{\mathrm{m}}, \tag{7}$$

where α and β are parameters of fitting.

Table 1 represents the parameters of fitting and the correlation coefficients for different temperatures. Parameters α and β are functions of temperature. The values of parameter α as a function of temperature were fitted by an exponential equation with correlation factor of 0.997:

$$\alpha = \alpha_{\mathrm{o}} + c\,\exp(dT), \tag{8}$$

where α_{o}, c, and d are 30.55 μS/cm, 3.3306×10^{-8} μS/cm, and 0.0598 K^{-1}. Parameter α increased exponentially with temperature due to the exponential decrease of viscosity. The temperature dependence of parameter β can be represented by

$$\beta = \beta_{\mathrm{o}} + f\,\exp(-gT), \tag{9}$$

where β_{o}, f, and g are 3,16,656.75 μS/cm, 96,48,593.64 μS/cm, and 0.0213 K^{-1}. The correlation factor of this equation was 0.996.

The ability of the resulting empirical equation to predict the EC of GO–distilled water nanofluid was evaluated by calculating the average of deviation percent which is defined as follows:

$$\text{Deviation percent} = \frac{\sigma_{\mathrm{cal}} - \sigma_{\mathrm{exp}}}{\sigma_{\mathrm{exp}}} \times 100, \tag{10}$$

where σ_{cal} and σ_{exp} represent the predicted and experimental EC of the nanofluid, respectively. The evaluated average deviation for EC of the present nanofluids was calculated to be 0.04 %.

A comparison between our work that was done for the first time on EC of GO-based nanofluid and some recent works on different carbonaceous nanofluids is shown in Table 2. It is outstandingly obvious that although the in-plane EC of GO is low, it provides significant enhancement in EC of the fluids in comparison with those of other works. The reason is that the surface charges of nanoparticles play an important role in increasing EC of the nanofluids, and there are high surface charges on GO nanosheets originating from its functional groups. Surprisingly, aqueous suspension of GO showed much higher EC enhancement in comparison with that of aqueous metal or metal oxide suspensions studied in our group (Azizi-Toupkanloo et al. 2014; Goharshadi and Azizi-

Table 1 Parameters and the correlation coefficients of linear equations of Eq. (7) for GO–distilled water nanofluids at different temperatures

T (°C)	α (μS/cm)	β (μS/cm)	R^2
25	32.320	333,228.571	0.9998
30	33.213	332,057.143	0.9991
35	33.980	330,200.000	0.9989
40	34.667	328,857.143	0.9991
45	38.107	327,457.143	0.9992
50	38.533	326,571.429	0.9992
55	41.953	325,228.571	0.9988
60	45.160	324,828.571	0.9988

Table 2 EC enhancement of different carbonaceous nanofluids

Nanomaterial	Base fluid	EC enhancement (%)	Concentration	Temperature	Ref.
Multiwalled CNT	Distilled water	~25	3 wt%	25 °C	Glory et al. (2008)
Sulfonated CNT	Deionized water: EG (50:50)	1,200	0.5 wt%	25 °C	Glover et al. (2008)
Functionalized graphene	Deionized water	1,400	0.03 vol%	25 °C	Baby and Ramaprabhu (2010)
Functionalized graphene	EG: distilled water (70:30)	8,620	0.395 vol%	30 °C	Kole and Dey (2013)
Functionalized graphene	Silicone oil	1,400	0.07 wt%	25 °C	Ma et al. (2013)
Graphene nanoplatelet	Distilled water	950	0.1 wt%	25 °C	Mehrali et al. (2014)
GO	Distilled water	25,678	0.06 wt%	25 °C	Present study

Toupkanloo 2013a) and other scientific groups (Ganguly et al. 2009; Minea and Luciu 2012).

Rheological behavior

The rheological properties of suspensions are governed by different factors. It is therefore necessary to investigate the rheology of GO–EG nanofluids at various mass fractions, temperatures, and shear rates. The viscosity of EG at 25 °C and shear rate of 27.5 s^{-1} was 16.5 cP which is in agreement with literature value (16.1 cP) (Lide 2000).

The viscosities of EG and GO–EG nanofluids as functions of shear rate at 25 °C are plotted in Fig. 6a. As the figure shows, the viscosity of nanofluids decreased non-linearly with increasing shear rate, indicating the strong "shear-thinning" behavior at low shear rates.

This shear-thinning behavior becomes more pronounced at the higher GO concentrations due to the stronger sheet–sheet and multi-sheet interactions with the increase in concentrations. Figure 6a shows that the viscosity of the nanofluid was higher than that of the base fluid. By increasing the concentration of GO in a suspension, the system becomes progressively chaotic as more aggregates form and viscosity increases. As the shear rate increases, the individual particles of aggregate start to break apart and align in the direction of the shearing flow and hence, the viscosity decreases. Therefore, the GO–EG nanofluids exhibited an obvious non-Newtonian shear-thinning behavior at low shear rates. The viscosity of nanofluid tended to reach a Newtonian plateau at high shear rates.

Figure 6b shows the viscosity of GO–EG nanofluid versus shear rate at different temperatures. Over the measured temperature range, viscosity of the nanofluid decreased with increasing shear rate. This non-Newtonian behavior was more obvious at low temperatures. At higher temperatures, the breakage of the nanoparticle aggregates leads the viscosity be independent of shear rate. This figure also shows that the viscosity of nanofluids decreased with an increase in temperature.

The values of η_{nf}/η_{bf}, defined as ratio of nanofluid viscosity, η_{nf}, to the viscosity of the base fluid, η_{bf}, under the same conditions are summarized in Table 3. By increasing mass fraction of GO nanosheets, the η_{nf}/η_{bf} increased for all shear rates and temperatures. As the mass fraction increased from 0.001 to 0.005 at 50 °C under shear rate of 67.5 s^{-1}, the η_{nf}/η_{bf} increased from 1.52 to 2.34. The η_{nf}/η_{bf} decreased from 1.53 to 1.45 by increasing shear rate from 90 to 115 s^{-1} which confirms the shear-thinning feature of nanofluids. This shear-thinning behavior is more prominent at low temperatures, high mass fractions, and low shear rates.

Different empirical equations have been proposed in the literature to predict the temperature dependence of viscosity of nanofluids (Kole and Dey 2010). Here, the viscosity of the base fluid and the GO–EG nanofluids was found to fit well with the Vogel–Tammann–Fulcher (VTF) equation (Goharshadi et al. 2013):

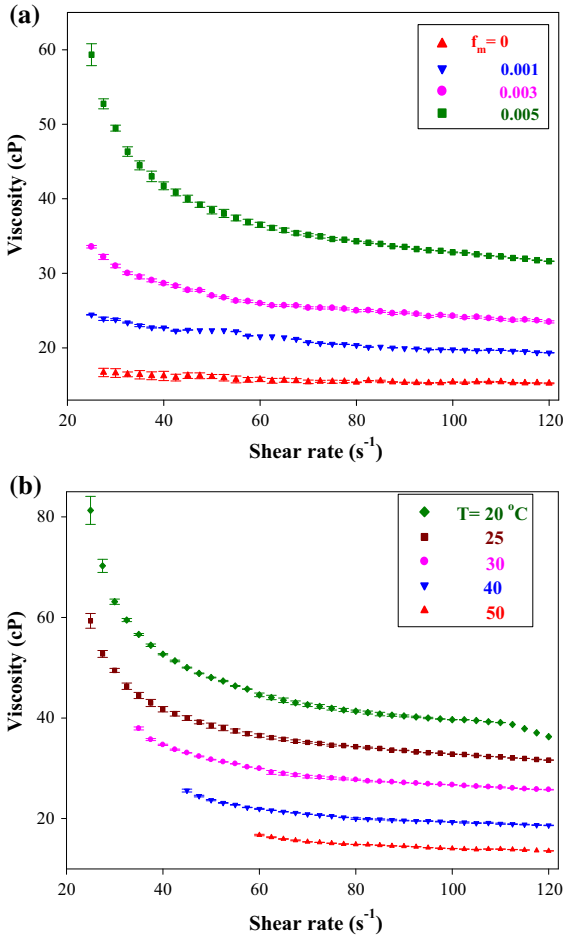

Fig. 6 The viscosity of **a** GO–EG nanofluids as a function of shear rate at 25 °C, and **b** GO–EG nanofluid as a function of shear rate at different temperatures with mass fraction of 0.005

$$\eta = A \exp\left(\frac{B}{T + C}\right), \tag{11}$$

where A, B, and C are constants. The three parameters in Eq. (11) have clear physical meanings: A is the value of η at the infinite temperature. B corresponds to the energy barrier associated with the so-called cage confinement due to the close packing of liquid molecules. C represents the temperature at which viscosity becomes infinite. It is also called zero-mobility temperature at which the free volume or configurational entropy of the liquid would vanish (Goharshadi et al. 2013). The experimental data at constant shear rate (80 s^{-1}) were fitted by Eq. (11) (Fig. 7). The fitting parameters and the correlation coefficients between the equation and measured values of the viscosity of nanofluids at different mass fractions are summarized in Table 4.

Table 3 The values of η_{nf}/η_{bf} at different temperatures and mass fractions under constant shear rates

Shear rate (s^{-1})	T(°C)	η_{nf}/η_{bf}		
		$f_{m\ =\ 0.001}$	0.003	0.005
67.5	20	1.37	1.60	2.27
	25	1.34	1.64	2.27
	30	1.39	1.64	2.28
	40	1.44	1.73	2.32
	50	1.52	1.85	2.34
90	20	1.31	1.53	2.17
	25	1.30	1.61	2.18
	30	1.39	1.62	2.22
	40	1.42	1.69	2.22
	50	1.49	1.76	2.18
115	20	1.26	1.45	2.03
	25	1.28	1.56	2.10
	30	1.35	1.58	2.11
	40	1.39	1.64	2.12
	50	1.44	1.71	2.08

Thermal conductivity

TC of GO–EG nanofluid, k_{nf}, was measured at different mass fractions and various temperatures (Fig. 8a). As the figure shows, the TC of EG and nanofluids increased linearly with raising temperature. The TC of the base fluid, k_{bf}, was 0.249 Wm^{-1} K^{-1} at 25 °C. At low mass fractions of GO (0.001 and 0.005), there was no significant enhancement in the TC of the nanofluids with respect to the base fluid. As the mass fraction increased to 0.01, the TC increased to about 0.259 Wm^{-1} K^{-1} at 25 °C because of the connection between the nanosheets (Baby and Ramaprabhu 2011).

The TC enhancement of nanofluids was calculated using the following equation:

$$\text{TC enhancement}\% = \frac{(k_{nf} - k_o)}{k_o} \times 100. \tag{12}$$

The TC enhancement of GO–EG nanofluids as a function of temperature and mass fraction is shown in Fig. 8b. The TC enhancement showed approximately

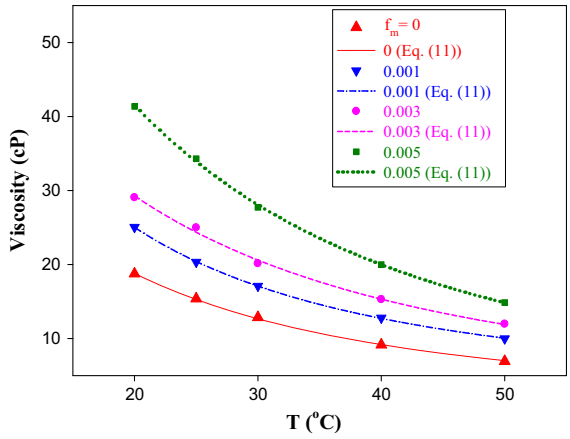

Fig. 7 Viscosity of GO–EG nanofluids as a function of temperature at a constant shear rate (80 s^{-1}), the *symbols* and *lines* are the measured and calculated values using Eq. (11), respectively

Table 4 The empirical constants of Eq. (11) and the correlation factors at different mass fractions under constant shear rate ($80s^{-1}$)

f_m	A	B	C	R^2
0	0.418	321.63	64.53	0.999
0.001	1.258	204.274	48.307	1
0.003	0.480	439.730	86.960	0.997
0.005	0.164	727.262	111.369	0.999

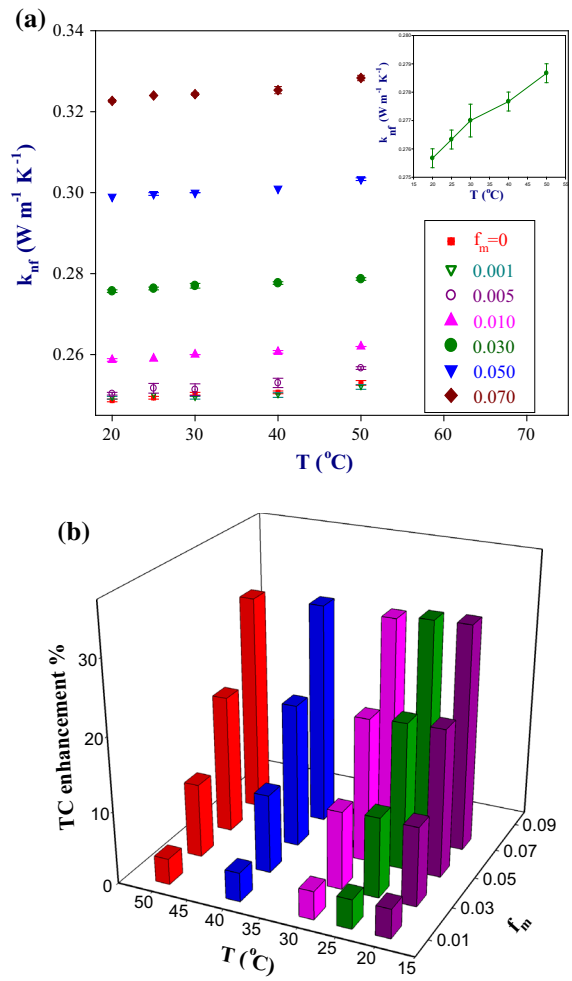

Fig. 8 **a** TC of EG and GO–EG nanofluids as a function of temperature at different mass fractions. The *error bars* are not visible because of large range of *y*-axis. The *inset* shows the TC of nanofluid with mass fraction of 0.03 versus temperature. **b** TC enhancement of GO–EG nanofluids both as a function of temperature and mass fraction

a linear increase with GO concentration. The maximum enhancement of ca. 30 % was observed for GO–EG nanofluid with mass fraction of 0.07. As the temperature increased, the TC of GO–EG nanofluid increased, while TC enhancement was being almost constant with raising temperature. Similar trend was reported by Yu et al. (2010a) for GO–EG nanofluids.

Many researchers found that the TC enhancements of nanofluids obviously increase with increase in temperature. Most of them proposed that Brownian motion of nanoparticles and the micro-convection caused by Brownian motion could explain the mechanism of TC enhancement (Jain et al. 2009; Jang and Choi 2004). However, as shown in Fig. 8b, the temperature exhibited no influence on the TC enhancements of GO–EG nanofluids in our work implying that the Brownian motion and micro-convection were not the dominant heat transfer mechanisms. The geometry of GO with high surface area and sheet-like structure is conducive for chain formation and percolation network structure (Wang et al. 2012a). The formation of a low-resistance heat flow percolation paths in the liquid could possibly explain the TC enhancement of GO–EG nanofluids.

Some research groups (Kole and Dey 2013; Yu et al. 2011) found that the experimental data of thermal conductivity of nanofluids containing nanosheets were in good agreement with the model developed by Nan et al. (1997). According to Nan's model, the TC of the nanofluid is expressed as

$$k_{nf} = k_{bf}\frac{3+\phi[2\beta_{11}(1-L_{11})+\beta_{33}(1-L_{33})]}{3-\phi(2\beta_{11}L_{11}+\beta_{33}L_{33})}, \quad (13)$$

where ϕ and L_{ii} are volume fraction and geometrical factor, respectively. For GO, the aspect ratio is very high, so $L_{11} = 0$ and $L_{33} = 1$ (Yu et al. 2011). β_{ii} is defined as

$$\beta_{ii} = \frac{k_p - k_{bf}}{k_{bf} + L_{ii}(k_p - k_{bf})}, \quad (14)$$

where k_p is the TC of the particles. As Fig. 9 shows, the TC proposed by Nan's model can be matched to the experimental results very well. Based on Eq. (13), using least square fitting of the experiment data, the in-plane thermal conductivity of GO was found to be 3.77 ± 0.09 Wm^{-1} K^{-1}. Using Nan's model, Yu et al. (2011) also estimated the in-plane thermal conductivity of GO to be 4.9 ± 0.6 Wm^{-1} K^{-1}. Such a low value for TC of GO was possibly due to significant amount of structural defects introduced during the chemical oxidation of graphite to GO. These defects promote phonon scattering effects and result in low thermal conductivity of GO (Yu et al. 2011). Furthermore, based on theoretical calculations (Nika et al. 2009), the TC depends strongly on the size of nanosheets and the edge roughness.

A linear regression analysis was also employed to develop an empirical relationship between TC of GO–EG nanofluids and mass fraction of GO nanosheets at different temperatures:

$$k_{nf} = af_m + b, \quad (15)$$

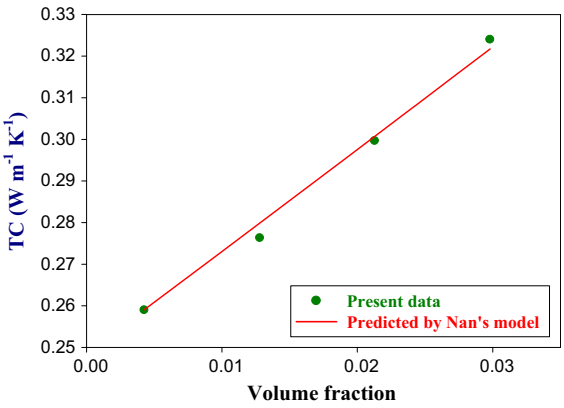

Fig. 9 TC of prepared nanofluids based on Nan's model (Nan et al. 1997) and experimental data at 25 °C

where a and b are the parameters of fitting. Table 5 shows the parameters and related correlation coefficients for different temperatures.

Conclusions

In summary, GtO was prepared via modified Hummers' method. It was successfully dispersed in distilled water and EG as the base fluids. One of the outstanding features of this work is that stable GO nanofluids were prepared via a simple way without requiring expensive surfactants or any special rigorous processes. The stability of the prepared nanofluids was investigated by UV–Vis spectroscopy and zeta potential measurement.

The transport properties, i.e., EC, viscosity, and TC of the nanofluids, were measured as functions of GO concentration and temperature. The main conclusions are as follows:

- The EC of GO–distilled water nanofluids was investigated for the first time. It was showed that the EC increased with increasing both mass fraction and temperature. An enormous enhancement of about 25,678 % was obtained (for mass fraction of 0.0006) which was much higher than those of other carbonaceous materials, metals, or metal oxides.
- The viscosity of nanofluids decreased significantly with increasing temperature, while it increased with increasing mass fraction. The maximum viscosity of GO–EG nanofluid, 81.29 cP, was obtained at 20 °C for 0.005 mass fraction of GO nanosheets (under shear rate of 25 s^{-1}). The nanofluids revealed shear-thinning behavior at low shear rates. The viscosity became constant at high shear rates because the interactions in the nanofluid became weak and the fluid aligned in the direction of the shearing flow.

Table 5 The parameters of Eq. (15) and the correlation coefficients

T (°C)	a (Wm^{-1} K^{-1})	b (Wm^{-1} K^{-1})	R^2
20	1.050	0.247	0.996
25	1.063	0.248	0.995
30	1.049	0.249	0.995
40	1.058	0.249	0.995
50	1.073	0.251	0.992

- Maximum of ca. 30 % enhancement in TC was achieved for GO–EG nanofluid with mass fraction of 0.07 for all temperatures. The TC enhancement of GO–EG nanofluids was almost constant with temperature.

The results obtained in the present work can provide better understanding of the transport properties of the GO dispersions for the different application areas such as conductive ink, coatings, and electronic and cooling industries.

Acknowledgments The authors would like to express their gratitude to Ferdowsi University of Mashhad for support of this project (Grant no. 3/29228).

References

Abareshi M, Goharshadi EK, Mojtaba Zebarjad S, Khandan Fadafan H, Youssefi A (2010) Fabrication, characterization and measurement of thermal conductivity of Fe_3O_4 nanofluids. J Magn Magn Mater 322:3895–3901. doi:10.1016/j.jmmm.2010.08.016

Acik M, Chabal YJ (2012) A review on reducing graphene oxide for band gap engineering. J Mater Sci Res 2:101

Amato G (1991) A new approach in the optical characterization of amorphous hydrogenated silicon-carbon alloys. Phys Status Solidi (b) 165:623–634

Azizi-Toupkanloo H, Goharshadi EK, Nancarrow P (2014) Structural, electrical, and rheological properties of palladium/silver bimetallic nanoparticles prepared by conventional and ultrasonic-assisted reduction methods. Adv Powder Technol 25:801–810. doi:10.1016/j.apt.2013.11.015

Baby TT, Ramaprabhu S (2010) Investigation of thermal and electrical conductivity of graphene based nanofluids. J Appl Phys 108:124308. doi:10.1063/1.3516289

Baby TT, Ramaprabhu S (2011) Synthesis and nanofluid application of silver nanoparticles decorated graphene. J Mater Chem 21:9702–9709. doi:10.1039/c0jm04106h

Boukhvalov DW, Katsnelson MI (2008) Modeling of graphite oxide. J Am Chem Soc 130:10697–10701. doi:10.1021/ja8021686

Brodie B (1860) Sur le poids atomique du graphite. Ann de chim et de phys 59:466–472

Cancado L et al (2006) General equation for the determination of the crystallite size L_a of nanographite by Raman spectroscopy. Appl Phys Lett 88:163106

Carrique F, Ruiz-Reina E (2009) Electrical conductivity of aqueous salt-free concentrated suspensions. Effects of water dissociation and CO_2 contamination. J Phys Chem B 113:10261–10270

Chakraborty S, Padhy S (2008) Anomalous electrical conductivity of nanoscale colloidal suspensions. ACS Nano 2:2029–2036. doi:10.1021/nn800343h

Chen L, Xie H (2009) Silicon oil based multiwalled carbon nanotubes nanofluid with optimized thermal conductivity enhancement. Colloids Surf A 352:136–140

Chen S, Zhu J, Huang H, Zeng G, Nie F, Wang X (2010) Facile solvothermal synthesis of graphene–MnOOH nanocomposites. J Solid State Chem 183:2552–2557

Dimiev AM, Alemany LB, Tour JM (2012) Graphene oxide. Origin of acidity, its instability in water, and a new dynamic structural model. ACS Nano 7:576–588. doi:10.1021/nn3047378

Dong M, Shen LP, Wang H, Wang HB, Miao J (2013) Investigation on the electrical conductivity of transformer oil-Based AlN nanofluid. J Nano Mater 2013:7. doi:10.1155/2013/842963

El Achaby M, Arrakhiz FZ, Vaudreuil S, Essassi EM, Qaiss A (2012) Piezoelectric β-polymorph formation and properties enhancement in graphene oxide—PVDF nanocomposite films. Appl Surf Sci 258:7668–7677. doi:10.1016/j.apsusc.2012.04.118

Ganguly S, Sikdar S, Basu S (2009) Experimental investigation of the effective electrical conductivity of aluminum oxide nanofluids. Powder Technol 196:326–330

Glory J, Bonetti M, Helezen M, Mayne-L'Hermite M, Reynaud C (2008) Thermal and electrical conductivities of water-based nanofluids prepared with long multiwalled carbon nanotubes. J Appl Phys. doi:10.1063/1.2908229

Glover B, Whites KW, Hong H, Mukherjee A, Billups WE (2008) Effective electrical conductivity of functional single-wall carbon nanotubes in aqueous fluids. Synth Met 158:506–508. doi:10.1016/j.synthmet.2008.03.022

Goharshadi EK, Azizi-Toupkanloo H (2013a) Silver colloid nanoparticles: ultrasound-assisted synthesis, electrical and rheological properties. Powder Technol 237:97–101. doi:10.1016/j.powtec.2012.12.059

Goharshadi EK, Azizi-Toupkanloo H (2013b) Silver colloid nanoparticles: ultrasound-assisted synthesis, electrical and rheological properties. Powder Technol 237:97–101

Goharshadi EK, Hadadian M (2012) Effect of calcination temperature on structural, vibrational, optical, and rheological properties of zirconia nanoparticles. Ceram Int 38:1771–1777. doi:10.1016/j.ceramint.2011.09.063

Goharshadi EK, Ahmadzadeh H, Samiee S, Hadadian M (2013) Nanofluids for heat transfer enhancement–A review. Phys Chem Res 1:1–33

Goncalves G, Marques PA, Granadeiro CM, Nogueira HI, Singh M, Gracio J (2009) Surface modification of graphene nanosheets with gold nanoparticles: the role of oxygen moieties at graphene surface on gold nucleation and growth. Chem Mater 21:4796–4802

Hunter RJ (1981) Zeta potential in colloid science: principles and applications, vol 125. Academic press, London

Jain S, Patel H, Das S (2009) Brownian dynamic simulation for the prediction of effective thermal conductivity of nanofluid. J Nanopart Res 11:767–773. doi:10.1007/s11051-008-9454-4

Jang SP, Choi SUS (2004) Role of Brownian motion in the enhanced thermal conductivity of nanofluids. Appl Phys Lett 84:4316. doi:10.1063/1.1756684

Jung I et al (2009) Reduction kinetics of graphene oxide determined by electrical transport measurements and

temperature programmed desorption. J Phys Chem C 113:18480–18486. doi:10.1021/jp904396j
Kang D-W, Shin H-S (2012) Control of size and physical properties of graphene oxide by changing the oxidation temperature. Carbon Lett 13:39–43
Kolbe J, Arp A, Calderone F, Meyer EM, Meyer W, Schaefer H, Stuve M (2007) Inkjettable conductive adhesive for use in microelectronics and microsystems technology. Microelectron Reliab 47:331–334
Kole M, Dey T (2010) Thermal conductivity and viscosity of Al_2O_3 nanofluid based on car engine coolant. J Phys D 43:315501
Kole M, Dey TK (2013) Investigation of thermal conductivity, viscosity, and electrical conductivity of graphene based nanofluids. J Appl Phys. doi:10.1063/1.4793581
Krishnamoorthy K, Veerapandian M, Yun K, Kim S-J (2013) The chemical and structural analysis of graphene oxide with different degrees of oxidation. Carbon 53:38–49
Kumar CMP, Venkatesha TV, Shabadi R (2013) Preparation and corrosion behavior of Ni and Ni–graphene composite coatings. Mater Res Bull 48:1477–1483. doi:10.1016/j.materresbull.2012.12.064
Kumar PV, Bardhan NM, Tongay S, Wu J, Belcher AM, Grossman JC (2014) Scalable enhancement of graphene oxide properties by thermally driven phase transformation. Nat Chem 6:151–158. doi:10.1038/nchem.1820
Lee JW, Ko JM, Kim J-D (2012) Hydrothermal preparation of nitrogen-doped graphene sheets via hexamethylenetetramine for application as supercapacitor electrodes. Electrochim Acta 85:459–466. doi:10.1016/j.electacta.2012.08.070
Lerf A, He H, Forster M, Klinowski J (1998) Structure of graphite oxide revisited. J Phys Chem b 102:4477–4482
Li H, Zhao Q, Li X, Zhu Z, Tade M, Liu S (2013) Fabrication, characterization, and photocatalytic property of α-Fe_2O_3/graphene oxide composite. J Nanopart Res 15:1–11. doi:10.1007/s11051-013-1670-x
Lide DR (2000) CRC handbook of chemistry and physics, 74th edn. CRC Press, Boca Raton
Loh KP, Bao Q, Eda G, Chhowalla M (2010) Graphene oxide as a chemically tunable platform for optical applications. Nat Chem 2:1015–1024
Long D, Li W, Ling L, Miyawaki J, Mochida I, Yoon S-H (2010) Preparation of nitrogen-doped graphene sheets by a combined chemical and hydrothermal reduction of graphene oxide. Langmuir 26:16096–16102. doi:10.1021/la102425a
Ma W, Yang F, Shi J, Wang F, Zhang Z, Wang S (2013) Silicone based nanofluids containing functionalized graphene nanosheets. Colloids Surf A 431:120–126. doi:10.1016/j.colsurfa.2013.04.031
Malard LM, Pimenta MA, Dresselhaus G, Dresselhaus MS (2009) Raman spectroscopy in graphene. Phys Rep 473:51–87. doi:10.1016/j.physrep.2009.02.003
Marcano DC et al (2010) Improved synthesis of graphene oxide. ACS Nano 4:4806–4814. doi:10.1021/nn1006368
Maxwell JC (1904) A treatise on electricity and magnetism vol 1, 3rd edn. Clarendon, Oxford
Mehrali M, Sadeghinezhad E, Latibari ST, Kazi SN, Mehrali M, Zubir MNBM, Metselaar HSC (2014) Investigation of thermal conductivity and rheological properties of nanofluids containing graphene nanoplatelets. Nanoscale Res Lett 9:1–12
Minea A, Luciu R (2012) Investigations on electrical conductivity of stabilized water based Al_2O_3 nanofluids. Microfluid Nanofluid 13:977–985. doi:10.1007/s10404-012-1017-4
Moghaddam MB, Goharshadi EK, Entezari MH, Nancarrow P (2013) Preparation, characterization, and rheological properties of graphene–glycerol nanofluids. Chem Eng J 231:365–372
Moosavi M, Goharshadi EK, Youssefi A (2010) Fabrication, characterization, and measurement of some physicochemical properties of ZnO nanofluids. Int J Heat Fluid Flow 31:599–605
Nan C-W, Birringer R, Clarke DR, Gleiter H (1997) Effective thermal conductivity of particulate composites with interfacial thermal resistance. J Appl Phys 81:6692. doi:10.1063/1.365209
Nika DL, Pokatilov EP, Askerov AS, Balandin AA (2009) Phonon thermal conduction in graphene: role of umklapp and edge roughness scattering. Phys Rev B 79:155413
Park S, Ruoff RS (2009) Chemical methods for the production of graphenes. Nat Nano 4:217–224
Patel H, Sundararajan T, Das S (2010) An experimental investigation into the thermal conductivity enhancement in oxide and metallic nanofluids. J Nanopart Res 12:1015–1031. doi:10.1007/s11051-009-9658-2
Pimenta M, Dresselhaus G, Dresselhaus MS, Cancado L, Jorio A, Saito R (2007) Studying disorder in graphite-based systems by Raman spectroscopy. PCCP 9:1276–1290
Radović M, Dohčević-Mitrović Z, Golubović A, Fruth V, Preda S, Šćepanović M, Popović ZV (2013) Influence of Fe^{3+}-doping on optical properties of CeO_{2-y} nanopowders. Ceram Int 39:4929–4936. doi:10.1016/j.ceramint.2012.11.087
Ruan B, Jacobi A (2012) Ultrasonication effects on thermal and rheological properties of carbon nanotube suspensions. Nanoscale Res Lett 7:1–14. doi:10.1186/1556-276X-7-127
Salehi J, Heyhat M, Rajabpour A (2013) Enhancement of thermal conductivity of silver nanofluid synthesized by a one-step method with the effect of polyvinylpyrrolidone on thermal behavior. Appl Phys Lett 102:231907
Sarojini KGK, Manoj SV, Singh PK, Pradeep T, Das SK (2013) Electrical conductivity of ceramic and metallic nanofluids. Colloids Surf A 417:39–46. doi:10.1016/j.colsurfa.2012.10.010
Shao G, Lu Y, Wu F, Yang C, Zeng F, Wu Q (2012) Graphene oxide: the mechanisms of oxidation and exfoliation. J Mater Sci 47:4400–4409
Shen L, Wang H, Dong M, Ma Z, Wang H (2012) Solvothermal synthesis and electrical conductivity model for the zinc oxide-insulated oil nanofluid. Phys Lett A 376:1053–1057
Shih C-J, Lin S, Sharma R, Strano MS, Blankschtein D (2011) Understanding the pH-dependent behavior of graphene oxide aqueous solutions: a comparative experimental and molecular dynamics simulation study. Langmuir 28:235–241
Solomon I, Schmidt MP, Sénémaud C, Driss Khodja M (1988) Band structure of carbonated amorphous silicon studied by optical, photoelectron, and x-ray spectroscopy. Phys Rev B 38:13263–13270

Sun L et al (2012) Nitrogen-doped graphene with high nitrogen level via a one-step hydrothermal reaction of graphene oxide with urea for superior capacitive energy storage. RSC Advances 2:4498–4506. doi:10.1039/C2RA01367C

Tesfai W, Singh P, Shatilla Y, Iqbal M, Abdala A (2013) Rheology and microstructure of dilute graphene oxide suspension. J Nanopart Res 15:1–7. doi:10.1007/s11051-013-1989-3

Tuinstra F (1970) Raman spectrum of graphite. J Chem Phys 53:1126. doi:10.1063/1.1674108

Wang B, Wang X, Lou W, Hao J (2012a) Thermal conductivity and rheological properties of graphite/oil nanofluids. Colloids Surf A 414:125–131. doi:10.1016/j.colsurfa.2012.08.008

Wang D-W, Du A, Taran E, Lu GQ, Gentle IR (2012b) A water-dielectric capacitor using hydrated graphene oxide film. J Mater Chem 22:21085. doi:10.1039/c2jm34476a

White SB, Shih AJ-M, Pipe KP (2011) Investigation of the electrical conductivity of propylene glycol-based ZnO nanofluids. Nanoscale Res Lett 6:1–5

Wojtoniszak M, Mijowska E (2012) Controlled oxidation of graphite to graphene oxide with novel oxidants in a bulk scale. J Nanopart Res 14:1–7. doi:10.1007/s11051-012-1248-z

Wu Z-S, Ren W, Gao L, Liu B, Jiang C, Cheng H-M (2009) Synthesis of high-quality graphene with a pre-determined number of layers. Carbon 47:493–499. doi:10.1016/j.carbon.2008.10.031

Yeganeh M, Shahtahmasebi N, Kompany A, Goharshadi E, Youssefi A, Šiller L (2010) Volume fraction and temperature variations of the effective thermal conductivity of nanodiamond fluids in deionized water. Int J Heat Mass Transf 53:3186–3192

Yin D et al (2013) Functional graphene oxide as a plasmid-based Stat3 siRNA carrier inhibits mouse malignant melanoma growth in vivo. Nanotechnology 24:105102

Yu W, Xie H, Bao D (2010a) Enhanced thermal conductivities of nanofluids containing graphene oxide nanosheets. Nanotechnology 21:055705

Yu W, Xie H, Chen W (2010b) Experimental investigation on thermal conductivity of nanofluids containing graphene oxide nanosheets. J Appl Phys 107:094317

Yu W, Xie H, Wang X, Wang X (2011) Significant thermal conductivity enhancement for nanofluids containing graphene nanosheets. Phys Lett A 375:1323–1328. doi:10.1016/j.physleta.2011.01.040